

Switching Strategies for Smart Fuses Based on Thermal Models of Different Complexity

Selcuk Önal, Anika Henke, Stephan Frei

On-board Systems Lab

TU Dortmund University

Otto-Hahn-Str. 4

44227 Dortmund, Germany

Email: selcuk.oenal@tu-dortmund.de

Abstract—In this paper, model-based approaches to control smart power-switches in vehicles are presented and discussed. The proposed methods use thermal cable models as well as the load characteristics to provide not only a cable protection with different switching strategies but also diagnosis functions such as virtual monitoring of thermal aging and dynamic load limits. Those can be implemented on microcontrollers in different levels of complexity depending on the needed accuracy and calculation speed.

Keywords — *electronic fuse, smart fuse, thermal cable model, radial heat transfer, axial heat transfer, approximation, switching strategies, temperature monitoring, load characteristic, RMS, cable aging*

I. INTRODUCTION

The complexity of automotive cable harnesses is continuously increasing due to higher demands for power and reliability. Therefore, new power net architectures are necessary [1]. Conventional melting fuses will not meet future demands anymore and will be successively replaced by smart power switches or “smart fuses” [2]. First applications are based on an integrated temperature monitoring of the power MOSFET which serves as main protection mechanism for cables. This way a specific thermal tripping characteristic similar to melting fuses but with smaller tolerances can be provided. Thus, a cross-section reduction is possible, depending on the load characteristic [3]. Some smart power switches also include protection mechanisms based on programmable overcurrent detection profiles but only in a simple manner for particular consumers like small dc motors or lamps [4]. However, the complexity of new power net architectures increases, and the electronic power switches become a crucial part of the power distribution nodes on system level. Especially, due to fail-safe and fail-operational functions towards autonomous driving, the smart power switches are intended not only to protect the cable but also to meet several diagnosis and controlling functions based on the monitoring of current, voltage as well as temperature. In

order to realize the relevant protection, diagnosis and controlling functions, the smart fuses have to be able to consider the thermal cable behavior as well as the permissible dynamic load characteristics. Here, depending on the complexity, different switching functions are conceivable.

Therefore, in this paper, at first, thermal cable models considering the radial and axial heat transfer for the estimation of the cable temperature are presented, which are needed to derive the basic tripping criterion for a model based smart fuse. As a tripping and diagnosis function, the calculation of the thermal aging of a cable based on the Arrhenius-Equation and also an approach for the online monitoring of the state of the load is presented. Different switching strategies are discussed with the help of an example. The proposed switching strategies will focus especially on the cable protection regarding fault tolerance and diagnosis functions in overloading situations of critical loads.

II. THERMAL MODELLING OF AUTOMOTIVE CABLES

Due to the high complexity of the installation conditions in a vehicle, such as bundle installation with multiple dynamic power losses, aging processes of contacts etc., the development of a reliable and accurate but still simple fuse-algorithm based on the radial or axial heat transfer is difficult. Since the real ambient conditions for cables, such as outside and local environmental temperatures as well as the laying situation, can vary strongly, worst-case assumptions must always be taken into account. In many automotive company standards such as LV112, a single cable hanging freely in air with a homogeneous maximum ambient temperature is assumed to be the worst-case scenario. Methods for temperature calculation will be presented now.

A. Radial Heat Transfer of a Single Cable

Assuming a very long (infinite) cylindrical cable in a homogeneous environment with constant current, then, a one-dimensional radial heat distribution fully describes the thermal behavior of the cable. The cross section of an isolated cable is shown in figure 1(a). The inner conductor (specific heat capacity c_c , thermal conductivity λ_c , radius r_c) has the temperature T_c and is surrounded by the insulation (specific heat capacity c_i , thermal conductivity λ_i , outer radius r_i). Due to the very high thermal conductivity of the conductor material (λ_c) in comparison to the insulating material (λ_i), the thermal resistance of the conductor can be neglected. The temperature at the surface of the insulation is T_s , whereas the ambient temperature is T_a . The heat source P'_{el} represents the electrical power dissipation caused by the electrical current I through the cable. The heat flow between the surface of the cable and the ambient air is called P'_α . To model the radial heat flow in this configuration, a thermal equivalent circuit with lumped elements as shown in figure 1(b) can be used.

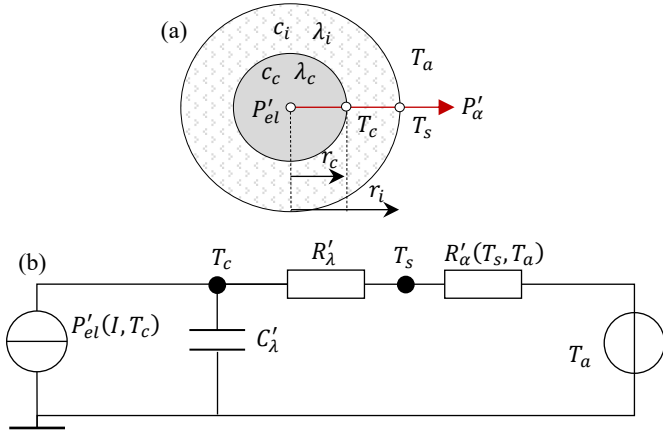


Fig. 1: (a) Cross section of the investigated cable. (b) Thermal circuit model for the radial heat transfer of a single core cable.

The parameters are given per unit length indicated by an apostrophe ($'$). The corresponding differential equation results as follows:

$$C'_\lambda \frac{dT_c(t)}{dt} = P'_{el}(I, T_c) - \frac{T_c(t) - T_a}{R'_\lambda + R'_\alpha(T_s, T_a)} \quad (1)$$

The heat source P'_{el} depends on the conductor temperature T_c via $P'_{el} = I^2 R'_{el}(T_c)$, where R'_{el} is the electrical resistance of conductor per meter and is given by

$$R'_{el} = R'_{ref} [1 + \alpha_T (T_c - T_{ref})]. \quad (2)$$

Here, R'_{ref} is the electrical resistance per unit length at the temperature T_{ref} , typically 20 °C, and α_T is the linear temperature coefficient of the conductor material.

The parameter C'_λ represents the overall thermal capacitance of the cable and is calculated via the specific heat capacities of the conductor and insulation material and

their volumes. R'_λ represents the thermal resistance through the insulation layer and is calculated with

$$R'_\lambda = \frac{\ln(r_i/r_c)}{2\pi\lambda_i}. \quad (3)$$

The heat transfer to the surrounding air by convection and radiation is considered by the thermal resistance R'_α , which is strongly temperature dependent:

$$R'_\alpha(T_s, T_a) = \frac{1}{\alpha(T_s, T_a) 2\pi r_i} \quad (4)$$

The parameter α considers the sum of the heat transfer coefficients describing convection (α_c) and radiation (α_r). For the calculation of these coefficients, the cable is assumed to be an infinite horizontal cylinder. Thus, the parametrization as well as the needed calculation is done according to [5]. Similar works can be found e.g. in [6] and [7]. Due to temperature dependency of R'_α , not only the conductor temperature T_c but also the surface temperature T_s has to be determined. Thus, applying modified nodal analysis (MNA) method on the basis of thermal circuit model in figure 1 and using implicit Euler method with a time step k and time step size Δt , gives the following equation for the calculation of the cable temperature:

$$T_c^{k+1} = \frac{(R'_\lambda + R'_\alpha) \cdot (C'_\lambda T_c^k + P'_{el} \Delta t) + \Delta t T_a^k}{C'_\lambda \cdot (R'_\lambda + R'_\alpha) + \Delta t} \quad (5)$$

P'_{el} can be determined via $(I^{k+1})^2 R'_{el}(T_c^k)$. The surface temperature T_s^{k+1} needed for $R'_\alpha(T_s^{k+1}, T_a^k)$ in (5), is calculated as follows:

$$T_s^{k+1} = \frac{R'_\alpha (C'_\lambda T_c^k + P'_{el} \Delta t) + (C'_\lambda \cdot R'_\lambda + \Delta t) T_a^k}{C'_\lambda (R'_\lambda + R'_\alpha) + \Delta t} \quad (6)$$

B. Axial Heat Transfer

If the axial power flow cannot be neglected, the radial heat transfer model is extended by the axial heat flow with corresponding thermal boundary conditions. In a first approximation, the axial heat transfer for a single cable in air with a worst-case parametrizing is considered. In order to indirectly consider the effect of a bundle installation, a thermal axial cable model can be also combined with indirect resistance measurements, as shown in [8]. In the following, a single cable placed freely in air is considered.

1) Numerical Approach

To consider the impact of the contacts on the temperature along the cable as well as different temperature zones, an axial discretization is needed for numerical treatment. The resulting model consists of several cable segments, as depicted in figure 2. Each segment is based on the thermal equivalent circuit shown in figure 1(b) considering the segment length $l_{seg,i}$ in the parameter calculations: The parameters are given no longer per unit

length, but they are calculated for the concrete segment length. The heat flow between adjoining segments takes place via thermal resistances between the corresponding heat sources. Thus, each segment has thermal resistances on both sides. Those are calculated using

$$R_{ax,i} = \frac{l_{seg,i}}{2\pi\lambda_c r_c^2}. \quad (7)$$

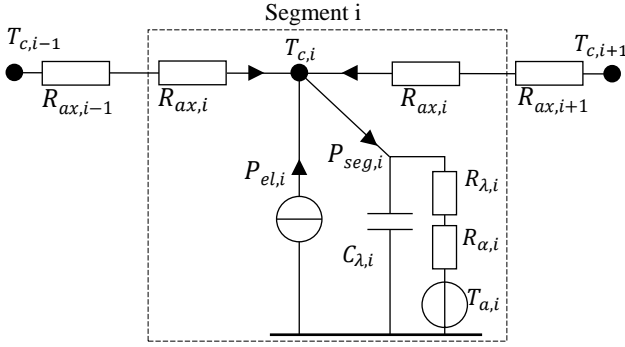


Fig. 2: Axial thermal segment model by discretization.

As with radial thermal model in the previous section, MNA method can be also applied to the entire cable. However, depending on the number of temperature nodes, it requires a higher computational effort. Instead, as an approximate solution, the conductor temperature can be also calculated individually for each segment according to equation (5) and (6), considering cable length in the calculations. Here, the electrical power loss has to be replaced with the total radial heat flow $P_{seg,i}$ for each segment as follows:

$$P_{seg,i}^{k+1} = (I^{k+1})^2 R_{el}(T_{c,i}^k) + \frac{T_{c,i-1}^k - T_{c,i}^k}{R_{ax,i-1}^k + R_{ax,i}^k} + \frac{T_{c,i+1}^k - T_{c,i}^k}{R_{ax,i+1}^k + R_{ax,i}^k}. \quad (8)$$

The index $i = 1$ indicates the first and index $i = n$ the last segment of the cable from left to right. In a first approximation, both cable ends are assumed to be ideal heat sinks, thus, their temperatures $T_{c,1}^k$ respectively $T_{c,n}^k$ are fixed. In this case, $R_{ax,i-1}^k$ respectively $R_{ax,i+1}^k$ are set to zero.

2) Analytical Approach

Some of the elements of the model presented in figure 1 are dependent on the temperature. For the analytical approximation that is presented in the following, these parameters are assumed to be constant using an average temperature for their calculation. Then, analogous to the description used for electrical transmission line theory, a circuit is derived, that describes an infinitely short section of the cable. For simplification, the axial resistances, that where split into two parts in section 1, are reduced to one

axial resistance per unit length here. The resulting model is shown in figure 3.

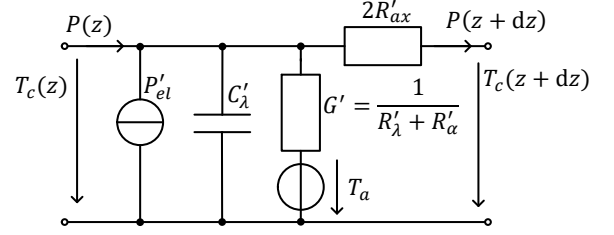


Fig. 3: Simplified thermoelectric equivalent model for a cable.

An inhomogeneous partial differential equation is derived from this model, which describes the temperature distribution along the cable:

$$\frac{1}{2R'_{ax}} \frac{d^2 T_c(z,t)}{dz^2} - G' T_c(z,t) - C'_{\lambda} \frac{dT_c(z,t)}{dt} = P'_{el} - G' T_a, \quad G' = \frac{1}{R'_{\alpha} + R'_{\lambda}}, \quad R'_{ax} = \frac{1}{2\pi\lambda_c r_c^2} \quad (9)$$

With $T_c(z, 0) = T_0 = \text{const.}$, $T_c(0, t) = T_1 = \text{const.}$ and $T_c(L, t) = T_2 = \text{const.}$ the Laplace transformation of the differential equation is done. Here, L is the length of the cable. In the Laplace domain, the solution is calculated:

$$T_c(z,s) = A_2 \exp\left(-z \sqrt{2R'_{ax}(G' + C'_{\lambda}s)}\right) + A_1 \exp\left(z \sqrt{2R'_{ax}(G' + C'_{\lambda}s)}\right) - \frac{P'_{el} - G' T_a - s C'_{\lambda} T_0}{s(G' + s C'_{\lambda})} \quad (10)$$

The factors A_1 and A_2 are derived using the remaining boundary conditions. The solution in the Laplace domain has to be transformed back into the time domain. Therefore, $A_1(s)$ and $A_2(s)$ are approximated by neglecting $\exp\left(-\sqrt{2R'_{ax}(G' + C'_{\lambda}s)} \cdot L\right)$ against ± 1 . The approximated result in the Laplace domain can be transformed back into the time domain analytically. With the resulting function, the temperature at each time and for each position along the cable is calculated independently. This analytical approximation, that does not take into account the temperature dependency of the parameters, provides fast information about the temperature along the cable for different times and positions. Special conditions as a constant ambient temperature, a constant current and fixed temperatures at the beginning and the end of the cable are assumed.

3) Investigation of the segment lengths and the initial temperature distribution for the numerical solution

Since the temperature of each segment is calculated separately under axial boundary conditions, the numerical calculation must be done in a row, e.g. from the left to the right cable end for each time step. Thus, for accurate results, the sampling time has to be high compared to the time scale of the radial heat transfer. To avoid higher

number of segments without a reduction of the accuracy, it is recommended to use an uneven distribution of segment lengths. The number of segments and the distribution of segment lengths has to be specified depending primarily on the cable lengths and the expected temperature gradients. Typically, a finer discretization at the cable's ends compared to the middle section of the cable is applied. To understand this, figure 4 shows the stationary calculated axial temperature profile for different cable cross-sections with an axial discretization of about 10 mm for the numerical solution as well as the results calculated using the analytical approximation. The deviations between both solutions are caused by the assumption in the analytical approach that the parameters of the equivalent circuit are constant. Each cable is loaded with a current leading to a cable temperature of about 105 °C in the stationary case for the ambient temperature 60 °C, respectively. The position "0 mm" represents the cable end with a fixed contact temperature of 60 °C. The temperature gradient is maximum at this point. The higher the distance to the cable end, the flatter the temperature profile becomes. After a specific distance from the cable end, e.g. 400 mm for the cross-section 2.5 mm², the middle section of the temperature profile is flat and coarse discretization is possible. The position "1000 mm" represents the center of the cable.

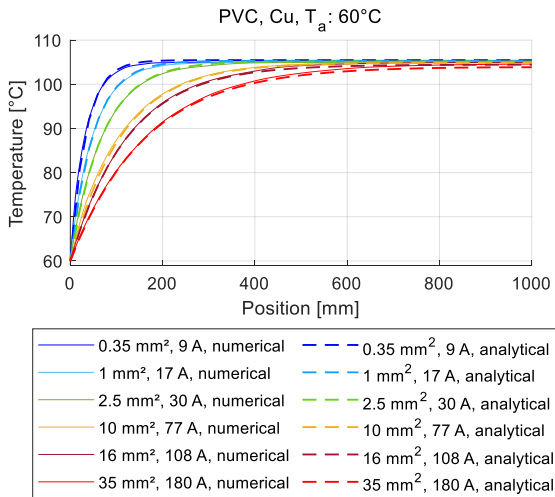


Fig. 4: Temperature gradients from cable end to the center.

Regarding the axial heat transfer of the cables, the initial conditions should be treated carefully in case of strongly differing temperatures of the ambient temperature zones or contacts. This is because the preset values typically will not meet a realistic temperature distribution for the initial state. To solve this problem, the needed initial conditions can be predetermined by simulation, as shown in figure 5. Additional to the numerical results, exemplary the temperature distribution based on the analytical approximation is shown for the time 1000 s, just before the cable is loaded with current.

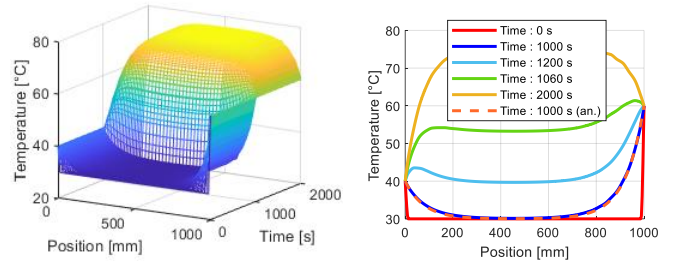


Fig. 5: Balancing of initial temperatures for the axial cable model: Simulation without any current from 0 s to 1000 s.

The examined 2.5 mm² cable has the fixed contact temperatures 40 °C respectively 60 °C and the ambient temperature 30 °C along the whole cable. A temperature balance is reached by simulation without current up to 1000 s, before the actual current (30 A) is applied. At this time point, the initial conditions for each segment can be extracted from the results (dark blue line or orange dashed line on the right plot).

III. SWITCHING AND DIAGNOSIS FUNCTIONS

In contrast to melting fuses, the switching conditions for smart fuses can be defined nearly arbitrarily. To illustrate this, figure 6 compares a typical dimensioning process in case of a melting fuse (a) and an electronic fuse (b) for an electric window lifter with the help of time current plots. To cover the worst-case, an ambient temperature of 60 °C is considered. As can be seen in figure 6(a), the suitable melting fuse and cable pair must be at least a 10 A blade fuse (ATO10) with a 0.75 mm² PVC cable without violating the normal operating region of the load. For the cable, depending on the required lifetime, both, the curves for a maximal temperature of 105 °C and of 155 °C are shown. The time current curve of the load is shown for a typical operation state obtained from moving average RMS filtering on the present current data. For the melting fuse, not only a typical time current curve from a manufacture datasheet but also tolerances according to ISO8820-3 are shown, which have to be taken into consideration as well. As can be seen, the characteristic of the melting fuse not only differs from that of the cable in its form but also it is affected by a big safety margin. Thus, an optimal matching of the time current characteristics for a melting fuse and cable pair is difficult, which is usually responsible for oversized cable cross-sections when using melting fuses for cable protection.

On the other hand, as figure 6(b) shows, the usage of a simple electronic fuse (red lines) with integrated thermal protection [3]. This could allow the reduction of the cable cross-section from 0.75 mm² down to 0.35 mm². However, depending on the application, the typical operating duration and cycles (see load limits in figure 6(b)) and environmental condition as well as the cooling surface area of the electronic fuse, the cross section 0.5 mm² might be an optimal choice. The final choice of the cable is often

based on previous development experience to increase the service life time of the cable. As highlighted by a red dotted line in figure 6(b), electronic fuses operate in saturation for higher currents leading to a limited current. If the load becomes more and more low ohmic, the current remains constant but the drain-source voltage increases. As a result, the electronic fuse switches off to protect itself. From, this current point, the time current characteristic of the electronic fuse in figure 6(b) illustrates only equivalent currents to show tripping times. Thus, for fully utilizing the potential of a cable, up to its limits without restriction of the operational area of load, it is necessary to oversize the electronic fuse over the cable and to use appropriate tripping algorithms. Doing this, the overall power net voltage and current stabilization has to be taken into account.

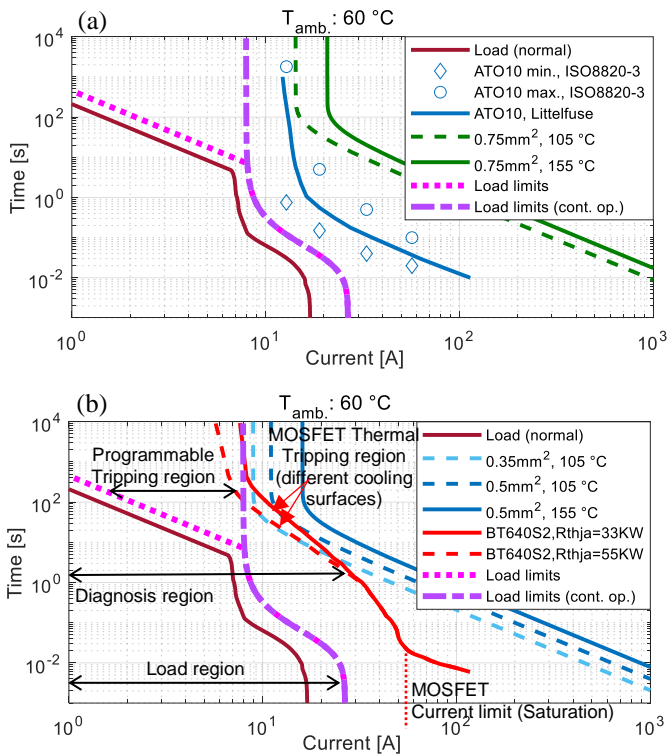


Fig. 6: Cross-section reduction and programmable fusing with smart fuses for an electric window ((a) conventional, (b) electronic fuse).

However, typical smart power switches already support a hardware-based output voltage monitoring as well as short-current detection. Therefore, in the following, different model-based switching strategies for the treatment of overload currents are addressed. In the next chapter, the strategies are proposed are tested by simulations using MATLAB-Simulink.

A. Temperature Monitoring

The standards ISO 6722 or LV112-1 define temperature classes and corresponding critical temperatures for typical insulation materials based on long-time aging under thermal stress, which can be used as tripping criterion.

As an example, in table I, the critical temperatures for the insulation material PVC with the temperature class B (105) are shown.

TABLE I: CRITICAL TEMPERATURES FOR PVC WITH TEMPERATURE CLASS B ACCORDING TO ISO 6722

Continuous operation temperature (3000 hours) T_{3000h} [°C]	Short-term temperature (240 hours) T_{240h} [°C]	Thermal overload (6 hours) T_{6h} [°C]
105	130	155

According to the data above, operating a PVC cable under 105 °C would lead to a critical thermal aging after 3000 hours, so that the cable insulation cannot fulfil the requirements anymore. The same already happens after only 6 hours, when the operation temperature is 155 °C. Therefore, it is crucial to consider operating periods and the corresponding duration of the load regarding the demanded lifetime. However, it has to be noted, that the cable temperature in the reality is likely to be lower than in calculation due to worst-case assumption. In case of cable protection, it is recommended to use the continuous operation temperature T_{3000h} as tripping criterion in most cases. However, distinguishing between critical and non-critical current paths or loads allows different strategies. In the following, two basic switching strategies based on the calculated cable temperature are addressed - simple switching-on/off depending on predefined temperature thresholds and holding the cable temperature under the critical value by providing an appropriate PWM duty cycle with the help of a control unit, as schematically shown in figure 7.

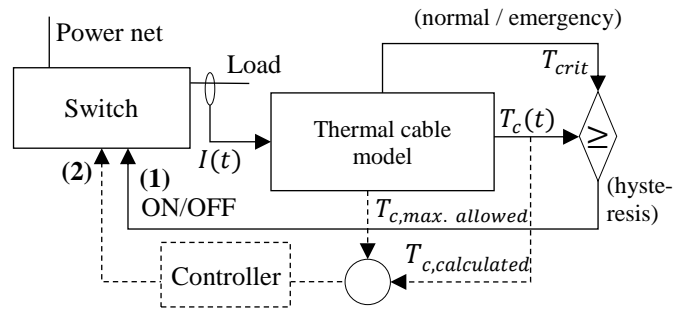


Fig. 7: Switching strategies based on the estimated cable temperature. (1) Simple ON/OFF switching. (2) Adjustment of PWM duty cycle.

Both strategies are based on the comparison of the model-based estimated temperature with a critical one but the change of the switch status differs. The first one (1) considers an ON/OFF-state depending on predefined temperature thresholds with a hysteresis enabling a resetting behavior. For critical consumers in the power net, especially in case of autonomous driving, an overcurrent should be tolerated as long as possible: As long as the power net voltage remains stable and the cable is still undamaged (T_{6h}), cable temperatures higher than T_{3000h} are

acceptable. Here, we recommend using T_{3000h} as threshold so that a hysteresis region between T_{3000h} and T_{6h} results as shown in figure 8(a). Thus, a kind of short-time fault tolerance without redundancy can be achieved.

The second strategy (2) considers an ohmic or inductive safety critical load, which is able to be controlled by a PWM voltage in case of faults or overloading instead of shutting-down. A corresponding controller has to provide the needed duty cycle for a desired temperature value $T_{c,desired}$. In [9], this approach is analyzed in detail for an ohmic and an inductive load. The main difficulties here are the nonlinearities resulting from the thermal behavior of the cable itself and the changes in the characteristics of the load in case of faults. Thus, a robust controller is necessary for a reliable application [9]. Here, it is reasonable to activate the PWM control also at T_{6h} in a safety critical case. A narrow hysteresis region to deactivate the PWM and regulating the temperature to a value slightly under T_{6h} can provide a good fault tolerance. Figure 8(b) illustrates this strategy. In the following we focus on the first strategy (1).

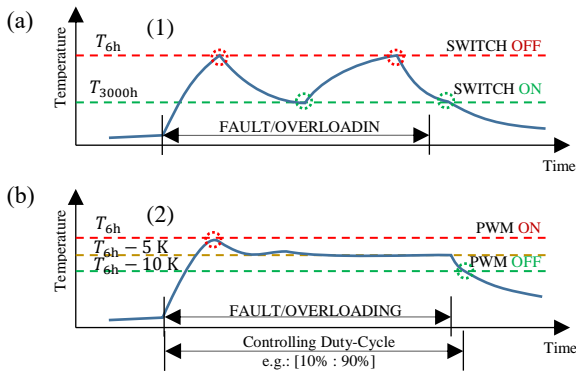


Fig. 8: Principle of switching strategies (1) and (2).

B. Monitoring of Thermal Cable Aging (State of Health)

In contrast to the melting fuses, with smart fuses it is more likely, that the cable is operated closely to its critical temperature. In this case, the aging process of the cable can significantly accelerate so that the cable insulation cannot meet the requirements after some time. To avoid this, the cable aging has to be estimated by the smart fuse and thus be used as additional switching criterion or for diagnosis. As a well-known approach, the aging time of the cable can be calculated on the basis of the Arrhenius-Equation [10], as shown in the following:

$$t_{aging} = Ae^{\frac{b}{T_c}} \quad (11)$$

A and b are insulation material-specific constants and T_c is the calculated conductor temperature in Kelvin. The constants A and b can be found via two pairs of the values t_{aging} and T_c . Using the temperatures T_{3000h} and T_{6h}

from table I leads to the following parameters for a cable with a PVC isolation:

$$A = 2.3219 \cdot 10^{-20} \text{ s}, \quad b = 2.0124 \cdot 10^4 \text{ K} \quad (12)$$

According to Miner's rule, it is possible to calculate the overall aging time of a cable under different temperatures by simply adding up the individual aging times [11]. Thus, a cumulative aging value in percent LT_{aging} can be expressed over time by integration over the aging speed $1/t_{aging}$ as follows:

$$LT_{aging}[\%] = 100 \cdot \int \frac{1}{A} e^{-\frac{b}{T_c(t)}} dt \quad (13)$$

Finally, the remaining life time in percent as *SoH* ("State of Health") of the cable can be calculated via $100 - LT_{aging}$ over the whole service time of the cable.

C. Load Monitoring (State of Load)

Vehicular power nets are designed and optimized during the development phase and the loads and their behaviors are well known. In most cases, a load can be described by a load characteristic as already exemplarily shown for an electric window in figure 6. Those load characteristics are primarily used for the evaluation of constant current pulses. When the current shows a transient development due to a very dynamic load such as an electric steering or multiple consumers on the same current path, equivalent constant current pulses can be calculated allowing the comparison with the load characteristic. Since the current is squared to obtain the power loss in the thermal domain, the obtained current profile is filtered by means of a moving RMS filter with different window lengths representing the length of current pulses in the load characteristic. Figure 9 graphically shows the use of this filtering method as a smart-fuse application, where a kind of dynamic load characteristic is observed. Here, the sample time of the current (a) as input directly represents the first current value for the load characteristic with a window length of the sample time. The square of the input current (b) is averaged with different windows lengths over time (c), so that each filter stage dynamically outputs, after extracting the root (d), the corresponding RMS current values for the load characteristic (e). These calculated RMS values are compared with reference values of a predefined load characteristic (f). Thus, it can be found, whether the load has left its operation region or not.

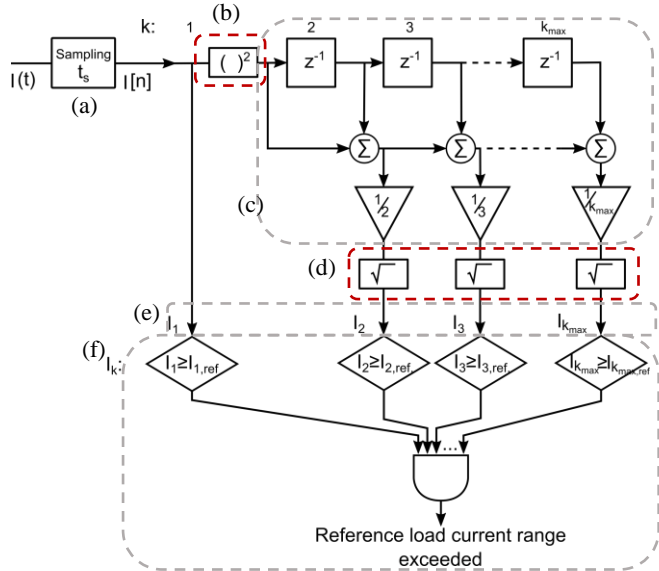


Fig. 9: Moving root mean square filter for load monitoring.

In the implementation of this filter, the square function at the input and the root function at each output stage, (see figure 9(b) respectively (d)) can lead to a high calculation effort. In the literature, there are several efficient computation methods to improve this [12].

Due to the wide logarithmic range in the time current characteristic (1 ms to 10,000 s), it is extremely inefficient to directly implement this filter on a microprocessor: It is necessary to reduce the order of the filter. For this purpose, the time axis in the time current data can be separated in time sections (subfilters) with different time steps, as proposed in table II.

TABLE II: PROPOSED TIME SECTIONS FOR THE MOVING RMS FILTER

Time section	1	2	3	4	5
Min. / Max Window Length	1 ms / 100 ms	110 ms / 1 s	1.1 s / 100 s	101 s / 1000 s	1010 s / 10000 s
Time step t_s	1 ms	10 ms	100 ms	1 s	10 s

For example, the first temperature section covers the filtering windows with a window length from 1 ms (sampling time at input) up to 100 ms and uses a time step of 1 ms. The second time section works with a time step of 10 ms in the area between 110 ms and 1 s. Thus, all relevant time regions in the time current characteristic (from 1 ms up to 10,000 s or approx. 2.8 hours) are covered with a total of 2980 time windows, so that the overall filter has the order 2980. It has to be noted, that in each time section except the first one, the input value represents the RMS value for the corresponding time step duration and has to be taken from a previous time section. For example, in time section 5, the time step is 10 s. Thus, every 10 seconds a new RMS filtered input current value has to be taken from the time section 3, where an RMS filtering with 10 s window length is already done.

In this paper, the proposed filter is implemented and tested in a MATLAB / Simulink environment. Here, we also implemented an additional function, to obtain a maximum percentage ratio of the calculated rms currents to the reference values from the load characteristic. We call this value *SoL* “State of Load”.

$$SoL [\%] = 100 \cdot \max_{k=\{1,2,\dots,k_{max}\}} \left[\frac{I_k}{I_{k,ref}} \right] \quad (14)$$

In a time critical environment, this additional function, which increases the calculation effort, could be omitted.

IV. APPLICATION EXAMPLE

For validation and demonstration of the proposed approaches, a simulation model is used, whose equivalent network is shown in figure 10. As a load we consider a dc motor based on the data of an electric window from the previous chapter. Here, we assume the motor to be a safety critical consumer for autonomous driving, whose operation has to be ensured as long as possible even under overload situations.

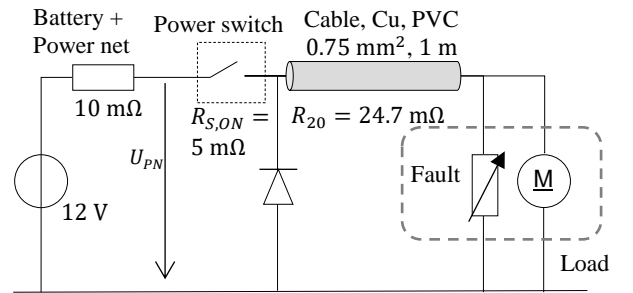


Fig. 10: Equivalent circuit for the application example.

Fault currents such as short time overloads are emulated by adding a variable resistance connected in parallel to the motor, as also depicted in figure 10. The motor current/voltage consumption can be described using the following transfer function $H_m(s)$.

$$H_m(s) = \frac{I_L(s)}{U_m(s)} = \frac{sJ + b}{(sJ + b) \cdot (sL_M + R_M) + k^2} \quad (15)$$

Here, J is the inertia, R_M is the resistance, L_M is the inductance of the motor and b is the motor viscous friction constant. k is a constant to consider the load torque M_L depending on the rotation speed ω_M with $M_L = k\omega_M$. The model is parametrized as follows:

$$\begin{aligned} R_M &= 600 \text{ m}\Omega, & L_M &= 800 \text{ }\mu\text{H}, \\ J &= 3 \cdot 10^{-6} \text{ kg} \cdot \text{m}^2, & K &= 10 \cdot 10^{-3} \text{ Vs/rad}, \\ b &= 90 \cdot 10^{-6} \text{ Nms/rad} \end{aligned} \quad (16)$$

Figure 11 shows the step response of the simulated motor current over time for a normal operation at 12 V and an overload operation at 14 V, which should be used to obtain the maximum load limits.

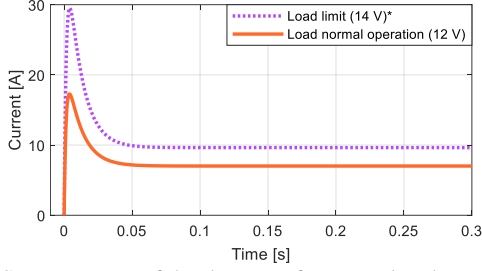


Fig. 11: Step-response of the dc motor for normal and overload operation (*For 14 V: $R_M = 400 \text{ m}\Omega$, $L_M = 600 \text{ }\mu\text{H}$, $J = 4 \cdot 10^{-6} \text{ kg} \cdot \text{m}^2$, $b = 95 \cdot 10^{-6} \text{ Nms/rad}$).

A. Tripping times

Figure 12 shows the corresponding load characteristic based on the motor current from figure 11 and the time current characteristic of the appropriate pair of the cable and the melting fuse, as already discussed in the previous chapter at a worst-case ambient temperature of $60 \text{ }^\circ\text{C}$. For the cable, the time current curve is depicted at the two different critical temperatures $T_{3000\text{h}} = 105 \text{ }^\circ\text{C}$ and $T_{6\text{h}} = 155 \text{ }^\circ\text{C}$. We consider a model-based smart fuse, that calculates the cable temperature and reproduces the given time current curves. Furthermore, we assume an optimal dimensioned power-switch and contact system, so that the cable can be fully utilized up to these temperature limits. A short-current limit is set, which must be far enough away from the worst-case load characteristic and provided by the integrated hardware in the power switch. Here, this limit, highlighted by a red line in figure 12, is set to 60 A , which leads to a maximum tripping time of about 5 s (up to $155 \text{ }^\circ\text{C}$). If the current is greater than 60 A , it is assumed, that an immediate short current switching-off is done by the hardware. For comparison, a typical time current characteristic of the corresponding melting fuse (ATO 10A) is considered via the datasheet of the manufacturer Littelfuse.

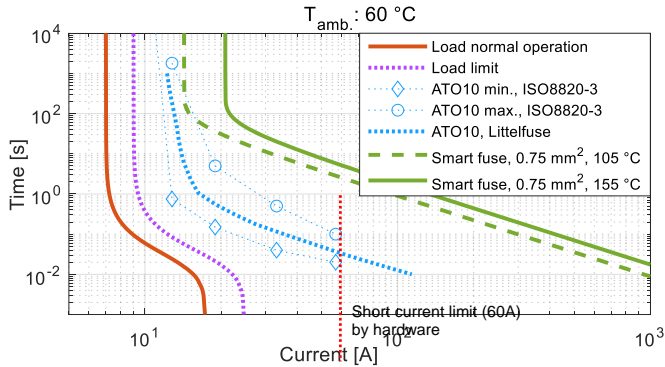


Fig. 12: Comparison of tripping and diagnosis times of a model based smart fuse with melting fuse.

The following table III shows the tripping times for some currents extracted from the time current characteristics in figure 12. The last column gives the time

to fail for long term aging assuming a continuous operation at the corresponding current. The column for the load limit shows when an overload current can be detected by a smart fuse, using the approach from the previous section.

TABLE III: COMPARISON OF THE TRIPPING/DIAGNOSIS TIMES. DERATING FOR THE AMBIENT TEMPERATURE $60 \text{ }^\circ\text{C}$.

I_L [A]	Melting fuse ATO 10A			Model based smart fuse			SoH 100 % \rightarrow 0 %
	min.	typ.	max.	Load limit	Cable 105 °C	Cable 155 °C	
9.4	∞	∞	∞	1 s	∞	∞	15 years
10.8	∞	∞	∞	0.2 s	∞	∞	5.7 years
12.8	0.75 s	190 s	1800 s	85 ms	∞	∞	1.2 years
18.96	0.15 s	0.56 s	5 s	21 ms	36.4 s	∞	38.9 h
33.18	40 ms	116 ms	0.5 s	1 ms*	9 s	16 s	48.9 s
56.87	20 ms	37 ms	100 ms	1 ms*	2.8 s	5.8 s	12.1 s
80	n.a.	19 ms	n.a.	1 ms*	**	**	5.9 s

* Limited by the sampling time for the current measurement
 ** Depending on a short current detection

As can be seen in table III, the tripping times of the melting fuses have a big range of tolerance without any diagnosis or controlling options. The typical melting times are very low although the cable has enough load reserves for overload situations. Using the time current characteristics of the cable gives the highest tripping times but also detecting of faults by load monitoring in shorter times than melting fuses. As already discussed in a previous chapter, the overload current leads to a reduced life time of the cable. This can be also monitoring by the SoH-value of the cable. Thus, the smart fuse can trip or provide diagnosis information depending on predefined limits.

B. Simulation with faults

As already described at the beginning of this chapter, the fault currents in the given application example should be emulated via a variable resistance in parallel to the motor (see figure 10). The resistance values R_{fault} over time used in the simulation is shown in figure 13. To keep the values recognizable in the plot, only the low impedance values are depicted, otherwise the resistance is high-ohmic. The resistance values (1) and (2) should lead to fault currents, which are only slightly above the load limits. The third one (3) should cause a load current which is noticeably higher than the load limit but is still tolerable by utilizing the available load reserve of the cable. The resistance values (4) and (5) are chosen to produce a higher power loss in the cable, so that the current has to be either limited or interrupted in order to protect the cable. The sixth one (6) represents a hard short-circuit, at which the current should immediately break at 60 A to protect the power switch itself and the overall power net.

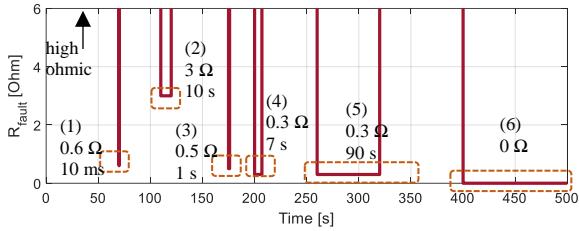


Fig. 13: Low impedance faults.

First, we take a look at the thermal behavior of the melting fuse using a thermal equivalent network and the corresponding parameters given in [13]. Figure 14(a) shows the total current resulting from the dc motor itself and the faults. The maximum permissible temperature of the melting fuse is 400 °C, as highlighted in figure 14(b). This temperature is already reached by the current pulse resulting from fault resistance (3) at the simulation time of 175 s. Thus, the current is interrupted within 120 ms, although the cable could tolerate this kind of short over-load current due to its higher thermal capacitance.

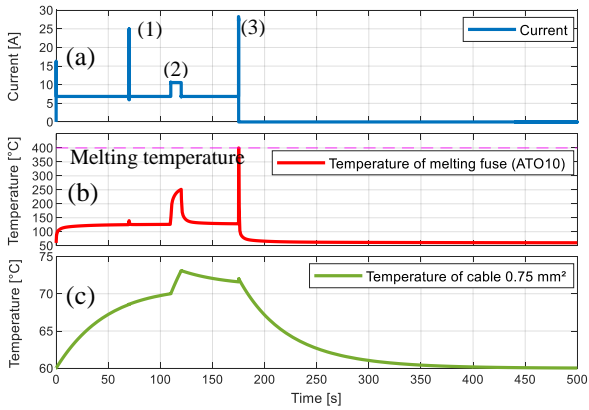


Fig. 14: Tripping behavior of the melting fuse (b) depending on the load current (a) in comparison with the cable temperature (c).

Figure 15 shows the results in case of a model based smart fuse. As can be seen in figure 15(d), the smart fuse detects fault currents (see figure 15(a)), resulting from fault resistances (1), (2) and (3), as the 100 % SoL-value is exceeded (see figure 15(d)). The cable temperature increases to a negligible level (see figure 15(c)). Since the load limit is reached, a higher level of control can decide, depending on the present driving situation, whether the current has to be interrupted or not and which temperature threshold has to be used. Here, a crucial driving case is considered, so that the smart fuse should tolerate these currents as far as possible and therefore sets the temperature threshold to the highest value of 155 °C instead of the normal value of 105 °C. Thus, the fault current (4) could be tolerated without interrupting the current. Here, a maximum cable temperature of ca. 126 °C has been reached. Between the simulation time of 260 s and 320 s, the cable temperature increases up to critical values due to fault resistance (5). Here, the smart fuse first switches off by

reaching the maximum allowed temperature of 155 °C at the time of about 270 s and then switches on, when the cable cools down below 105 °C after about 27 s. So, the motor is in operation at the time of 297 s again, despite the fault current. However, since the fault current is still present, a second switching-off takes place at the time of about 304 s. The fault current (4) is not present anymore from the time of 320 s, so that the smart fuse switches on when the cable temperature falls below 105 °C and the motor is in operation again.

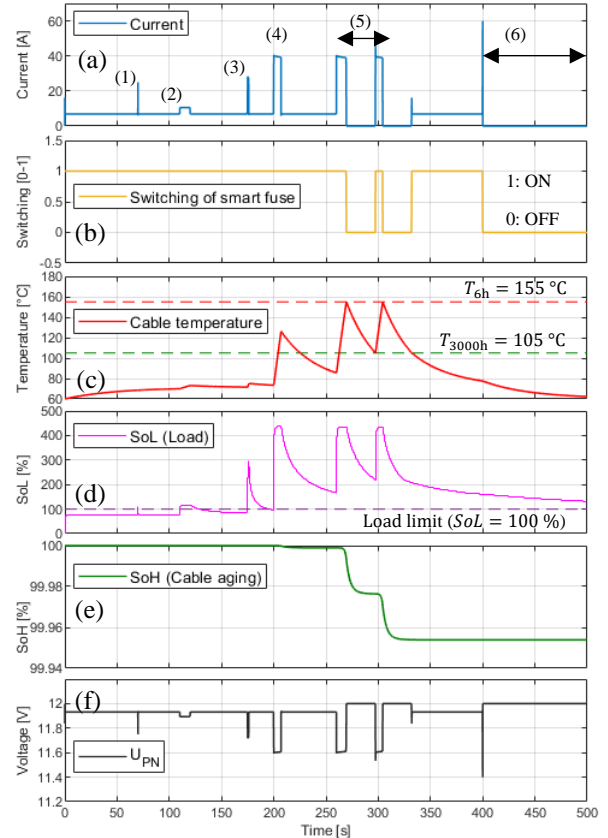


Fig. 15: Tripping behavior of a smart fuse.

Finally, a short circuit at the time of 400 s leads to an immediate switching-off by reaching the current limit 60 A. In figure 15(e), the monitoring of cable aging in percent can be seen. As figure 15(f) shows, the power net voltage (U_{PN}) remains stable. In this example, we assumed that the motor is still operable, as long as the fault current can be tolerated. Thus, it can be directly seen from switching signal of smart fuse in figure 15(b), that the motor is operable despite over-currents as long as the cable temperature remains below 155 °C and no short circuit is present. Using a PWM-Switching, where the cable temperature is regulated by changing the duty-cycle, can also keep the motor in operation, with a reduced performance, as discussed in chapter III.

V. CONCLUSION

In this paper, model-based switching strategies for automotive smart fuses using the thermal characteristics of the cables and load characteristics have been discussed and analyzed by simulations. The proposed methods provide an adaptive adjustment of the switching behavior of smart fuses considering the resulting cable heating and load limits. Here, later tripping times have been reached in comparison with melting fuses without any damage of the cable. The online monitoring of the load by a moving RMS filtering as well as the monitoring of long-term cable aging provide diagnosis functions. Thus, the proposed model-based control methods for smart fuses offer several benefits compared to melting fuses as well as simple electronic fuses especially in fail-safe and fail-operational autonomous driving applications.

REFERENCES

- [1] D. Dieckhöfer, V. Hoffmann and U. Hornfeck, „Dezentrale Bordnetzarchitektur - Leistungsverteilung von morgen“, *ATZ-Elektronik*, vol. 11, no. 1, pp. 38-41, 2016.
- [2] X. Tian, N. Shen and X. Wang, “Study of Replacing the Traditional Electromechanical Relay with the Full Semiconductor Solution of Bussed Electrical Center”, *WCX SAE World Congress Experience*, United States, 2019.
- [3] A. Graf, “Smart Power Switches for Automobile and Industrial Applications”, *VDE, ETG Conference “Contact Performance and Switching”*, Karlsruhe, 2001.
- [4] S. Everson, “eSwitch: Design Considerations for Robustness and Reliability”, *Freescale Technology Forum*, 2009.
- [5] „VDI-Wärmeatlas“ Fachlicher Träger VDI-Gesellschaft Verfahrenstechnik und Chemieingenieurwesen, Springer, 2019.
- [6] T. Schulz, „Grundsatzuntersuchung zum Temperaturverhalten elektrischer Leitungen und deren Schutzelemente auf Schmelzleiterbasis in Kfz-Bordnetzen“, Düsseldorf, VDI Verlag, 2003.
- [7] A. Ilgevicus, “Analytical and numerical analysis and simulation of heat transfer in electrical conductors and fuses”, Neubiberg: Universität der Bundeswehr München, 2004.
- [8] S. Önal and S. Frei, “A model-based automotive smart fuse approach considering environmental conditions and insulation aging for higher current load limits and short-term overload operations”, *ESARS ITEC*, 2018.
- [9] H. Nguyen, “Modélisation électrothermique de système électrique électronique automobile et pilotage de mosfet intelligents pour protéger les faisceaux, éviter les courts circuits aggravés et diminuer la masse de câblage”, Dissertation, University of Bordeaux 1, 2013.
- [10] L. Heinhold, “Power cables and their application, Pt. 1”, SIEMENS, Berlin, Germany, 1979.
- [11] Y. J. Han, H. M. Lee and Y.-J. Shin, “Thermal Aging Estimation with Load Cycle Thermal Transients for XLPE-insulated Underground Cable”, *IEEE Conference on Electrical Insulation and Dielectric Phenomenon (CEIDP)*, 2017.
- [12] B. Neunaber, “Improve your root-mean calculations”, *EE Times-India*, 2006.
- [13] P. Schwarz, J. Haase, "Erstellung einer VHDL-AMS Modellbibliothek für die Simulation von Kfz-Systemen," *FAT* Schriftenreihe, vol. FAT 207, 2006.